ARTICLE

Toward Single-Chirality Carbon Nanotube Device Arrays

Aravind Vijayaraghavan,[†,∥,*] Frank Hennrich,[†] Ninette Stürzl,[†,‡] Michael Engel,[†,§,⊥] Marc Ganzhorn,[†,§,#] Matti Oron-Carl,[†] Christoph W. Marquardt,[†,§] Simone Dehm,[†] Sergei Lebedkin,[†] Manfred M. Kappes,[†,‡,⊥] and Ralph Krupke[†,⊥,*]

[†]Institut für Nanotechnologie, Karlsruhe Institute of Technology, 76021 Karlsruhe, Germany, [‡]Institut für Physikalische Chemie, Karlsruhe Institute of Technology, 76021 Karlsruhe, Germany, [§]Physikalisches Institut, Karlsruhe Institute of Technology, 76021 Karlsruhe, Germany, and [⊥]DFG Center for Functional Nanostructures (CFN), 76028 Karlsruhe, Germany. [∥]Present address: Department of Chemical Engineering, Massachusetts Institute of Technology, Cambridge, Massachusetts 02139. [#]Present address: Institut Néel, CNRS-Université Joseph Fourier-Grenoble INP, BP 166, 38042, Grenoble, France.

ABSTRACT The large-scale integration of devices consisting of individual single-walled carbon nanotubes (SWCNT), all of the same chirality, is a critical step toward their electronic, optoelectronic, and electromechanical application. Here, the authors realize two related goals, the first of which is the fabrication of high-density, single-chirality SWCNT device arrays by dielectrophoretic assembly from monodisperse SWCNT solution obtained by polymer-mediated sorting. Such arrays are ideal for correlating measurements using various techniques across multiple identical devices, which is the second goal. The arrays are characterized by voltage-contrast scanning electron microscopy, electron transport, photoluminescence (PL), and Raman spectroscopy and show identical signatures as expected for single-chirality SWCNTs. In the assembled nanotubes, a large D peak in Raman spectra, a large dark-exciton peak in PL spectra as well as lowered conductance and slow switching in electron transport are all shown to be correlated to each other. By comparison to control samples, we conclude that these are the result of scattering from electronic and not structural defects resulting from the polymer wrapping, similar to what has been predicted for DNA wrapping.

KEYWORDS: single-wall carbon nanotube · chirality · Raman spectroscopy · photoluminescence spectroscopy · directed assembly · polyoctylfluorenyl · defects

The structure−property correlation in single-walled carbon nanotubes (SWCNT)[1,2] and the resultant unique diversity in their electronic properties allows for the fabrication of devices that are superior in performance and functionality to silicon-based devices.[3,4] Depending on their chirality, SWCNTs are either metallic (zero band gap) or semiconducting, with band-gaps up to 1.5 eV. As grown semiconducting SWCNTs have a wide distribution of diameter and chirality resulting in a large variation in band gap. Therefore, without control over their structure, this diversity is also a major hurdle in terms of quality and reproducibility in large-scale device integration.[5] This polydispersity affects properties and limits application of SWCNTs across a wide range,[6] including field-effect transistors (FETs), interconnects, optoelectronic emitters/detectors, chemical sensors, and nanoelectromechanical resonators. Hence, the large-scale, efficient integration of SWCNTs of a single chirality and controlled length into lithographic circuits at specific locations has been identified as the most challenging and rewarding step toward a surge in the application of SWCNTs.[7]

We adopt a combination of single-chirality nanotube suspensions made by chirality-selective polymer wrapping with ultra-large scale directed assembly by dielectrophoresis as the route to fabricating high-density arrays of individual, single-chirality nanotube devices. Individual nanotubes incorporated in the device locations are imaged with voltage-contrast scanning electron microscopy (VC-SEM).[8] The single-chirality assembly is confirmed by Raman and photoluminescence (PL) spectroscopy. The device performance in three-terminal field-effect transistor configuration is also measured. This advancement is not only technologically significant, but also enables new scientific insights through cross-correlated measurements on individual, identical SWCNTs using different experimental techniques on a statistically significant number of devices. We demonstrate this by relating the high intensity of Raman D peak and PL dark-exciton (DE) peak with suppressed conductance and slow switching and attribute these to enhanced scattering at electronic defects related to the polymer wrapping.

Large-scale assembly of individual SWCNTs has been achieved by dielectrophoresis from an aqueous suspension.[9] The process is self-limiting to one nanotube per device. This is because the polarizability of the nanotube is high compared to the surrounding medium and the deposition

*Address correspondence to aravind.vijayaraghavan@kit.edu, ralph.krupke@kit.edu.

Received for review September 4, 2009 and accepted March 19, 2010.

Published online April 21, 2010. 10.1021/nn100337t

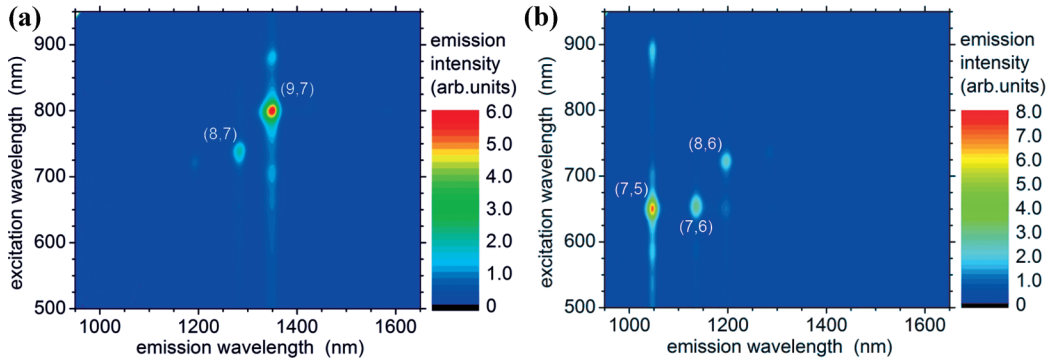

Figure 1. Two-dimensional PL contour maps (PL emission intensity versus excitation and emission wavelengths) of chirality-sorted SWCNT solutions: (a) ~90% (9,7) [also (8,7), (8,6)] and (b) ~50% (7,5) [also (7,6), (8,6), (8,7)] SWCNT suspensions. Compositions estimated from integrated peak intensities.

of the first nanotube in between the electrodes changes the dielectrophoretic force fields around it from attractive to repulsive and prevents the incorporation of further nanotubes in to the device. Dielectrophoretic assembly is scalable to competitive integration densities of 1 million devices per sq cm and beyond, limited only by the thickness of the underlying gate dielectric. The location, orientation, and channel lengths of the device are predefined. Dielectrophoresis is also, in itself, capable of sorting nanotubes by electronic type[10] and this along with length-sorting[11−13] would suffice to deposit metallic-only SWCNT devices.[14] Semiconducting SWCNTs, however, have to be additionally sorted by diameter and chirality and dielectrophoresis is limited by its inability to extract semiconducting SWCNTs or overcome the polydispersity problem. Therefore, it is required to resort to presorting by length, diameter, and chirality by a different method. Fortunately, deposition by dielectrophoresis is possible from a variety of different solvents and is independent of the nanotube source or processing steps they have undergone.

Recently, SWCNTs have been sorted into narrow diameter fractions by density gradient ultracentrifugation (DGU)[15,16] and repeated iterations of DGU can narrow the diameter distribution down to a single chirality for small-diameter SWCNTs.[17] Another method involves certain polymers[18,19] that selectively wrap around nanotubes of near-armchair chiralities. Similar chirality selectivity has also been shown for DNA wrapping[20,21] of nanotubes. These approaches all yield single-chirality suspensions of SWCNTs that are compatible with dielectrophoretic deposition.

RESULTS AND DISCUSSION

Monodisperse SWCNT Solution. Figure 1a,b shows the PL spectral maps of two source suspensions, with predominantly (9,7) and (7,5) chiralities, respectively. The polymer-wrapping method for extraction of single chiralities is used here because it yields the highest purity among available techniques. Devices fabricated from surfactant-stabilized, semiconducting, arc-discharge SWCNT suspension have higher-performance device characteristics[22] compared to the nanotubes used here. However, due to experimental limitations, we are unable to characterize such SWCNTs by optical spectroscopy; the detection range of an InGaAs detector is insufficient to record their PL spectra, and excitation for resonant Raman spectroscopy requires lasers of infrared wavelengths. Therefore, proof of assembly can only be obtained from electron transport measurements and they can also not be used to accomplish the second goal of correlated measurements. (9,7) and (7,5) SWCNTs, on the other hand, can be characterized by Raman and PL spectroscopy, in addition to transport measurements, to provide evidence for monodisperse device assembly and demonstrate correlated measurements across identical devices. The devices fabricated here have adequate performance for applications such as sensing, as will be demonstrated elsewhere, and superior device performance is only required for microelectronic applications targeted at replacing Si-FETs.

Voltage-Contrast Scanning Electron Microscopy. Figure 2 shows a representative region of the device array, con-

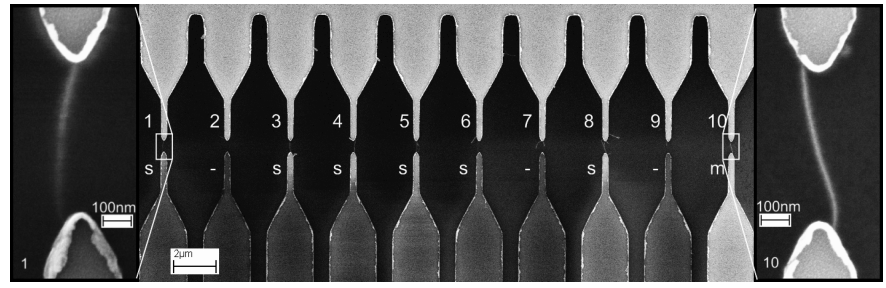

Figure 2. VC-SEM of an array of (9,7) SWCNT devices. Six devices are semiconducting (s) (1,3−6,8). These devices show gradual variation in contrast along their length, and the contrast of the source electrode lags behind the contrast of the drain, such as seen in device 1 (left inset). One device has a metallic (m) nanotube (10) showing uniform contrast along its length and a bright source electrode for all bias conditions, such as seen in device 10 (right inset). Three devices are not bridged (-) (2, 7, 9) because the nanotubes deposited there are too short.

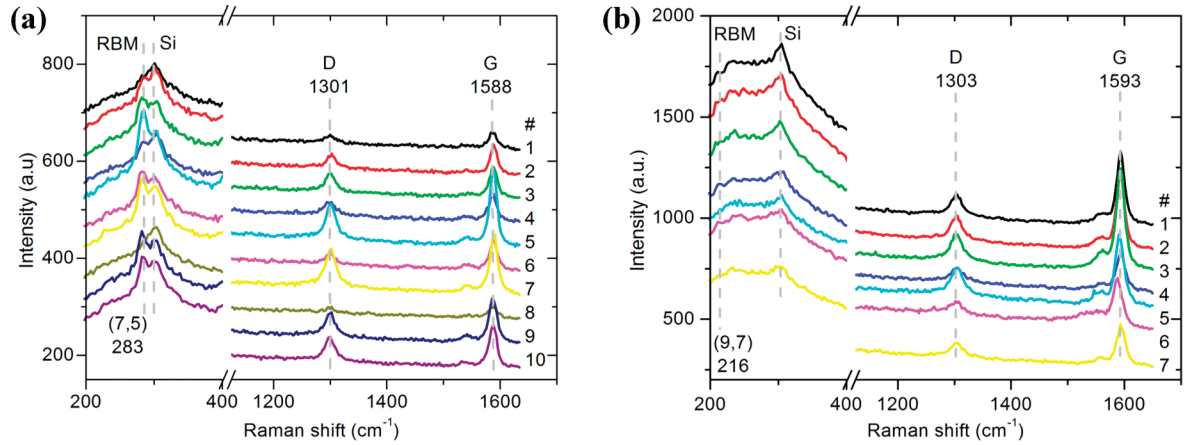

Figure 3. Raman spectrum of 10 successive devices in a (a) (7,5) SWCNT and (b) (9,7) SWCNT array measured at 633 nm excitation. The G, D, and Si peak (302 cm^{-1}) are observed for all devices. (a) Devices 2−7, 9, and 10 show characteristic RBM peak at 283 cm^{-1} and typical line shape of G-mode for semiconducting nanotubes, indicating that these are (7,5) nanotubes. All devices show Raman signal, including those that contain nanotubes that are too short to bridge the electrodes and form functioning devices. (b) No clear RBM signal, expected at 216 cm^{-1}, is observed, because the 633 nm excitation is not within the RBM resonance window of (9,7) SWCNTs. However, G- and D-modes are observed at all locations. Both arrays show unusually large D peaks.

sisting of 10 electrode pairs, of which seven are bridged by a nanotube. Of these, VC-SEM and transport measurements confirm that six are semiconducting SWCNT devices, while one is metallic. Semiconducting SWCNTs show a gradient in their contrast profile at low gate-bias conditions in VC-SEM, while metallic SWCNTs show a uniform contrast profile, as seen in the insets in Figure 2. This distribution of semiconducting, metallic, and unbridged devices is typical of the entire array. Supporting Information, Figure 3 shows the VC-SEM of a full 100 × 100 sq μm array of 100 devices deposited from the (9,7) nanotube suspension. Of these, 82 are successfully bridged and 70 of those are semiconducting.

All unbridged devices, on closer inspection, show nanotubes connected to one electrode but not bridging the gap. This is due to the significant number of nanotubes in the solution that are shorter than the electrode gap (Supporting Information, Figure 1b). The yield can be improved by narrowing the length distribution of nanotubes in solution, such as by size-exclusion chromatography[11] and density gradient ultracentrifugation.[12,13] The small fraction of metallic devices can be eliminated by improving the separation process.

Raman and Photoluminescence Spectroscopy. The presence of single-chirality SWCNTs at the individual device locations is confirmed by a combination of micro-Raman and micro-PL spectroscopy. Figure 3 shows the Raman spectra obtained on 10 adjacent devices on an array deposited from the (7,5) suspension and seven adjacent devices on an array deposited from the (9,7) suspension. The regions of interest, *i.e.*, radial breathing mode (RBM) and the D- and G-modes, are presented. We use 633 nm excitation, which is within the resonance window for D-mode, G-mode, and RBM scattering processes of (7,5) SWCNTs. In the (7,5) array, an RBM peak at 283 cm^{-1},[23] characteristic of the (7,5) nanotube, is seen in eight of these devices. The corresponding G peak is dominated by the tall and narrow higher energy G^+ peak at ∼1588 cm^{-1}, as expected for a semiconducting carbon nanotube.[24,25] The other two devices are semiconducting as well but do not have a characteristic RBM signal. This yield of semiconducting devices in the array is comparable to estimates from VC-SEM. The 633 nm excitation is also within the resonance window of the (9,7) SWCNTs for D- and G-mode Raman scattering processes but not for the RBM process. Hence, no clear RBM signal (expected at 216 cm^{-1})[23] is seen, while the G- and D-modes could be recorded, albeit at lower intensity. Note that, for the spectra presented in Figure 3, integration times of 5 and 60 s were used for the (7,5) and (9,7) SWCNT array, respectively. The G^+ peak for the (9,7) nanotubes at ∼1593 cm^{-1} is up-shifted compared to (9,7) nanotubes, as expected from the curvature effect.[26] Both the (9,7) and (7,5) SWCNTs exhibit an unusually large D-mode intensity. While the (7,5) SWCNT spectra serves to establish the assembly of single-chirality devices across the array using the signature RBM peak, the (9,7) SWCNT spectra serves to illustrate the correlation between spectral and electronic transport features discussed in subsequent paragraphs.

Figure 4a shows a typical PL spectral map of an individual device in an array deposited from the (9,7) suspension. The characteristic bright-exciton (BE) PL emission of a (9,7) nanotube, at 1345 nm under an 800 nm excitation, is seen along with the corresponding dark-exciton (DE1)[27] peak at 1540 nm, which was recently assigned to the phonon sideband of the *K*-momentum DE states above the lowest BE state.[28,29] In some devices, the weaker DE2 dark exciton peak of unclear origin can also be seen as a shoulder to the BE peak at 1365 nm. The red-shift of 120 and 15 meV for the DE1 and DE2 peaks with respect to the BE peak is consistent

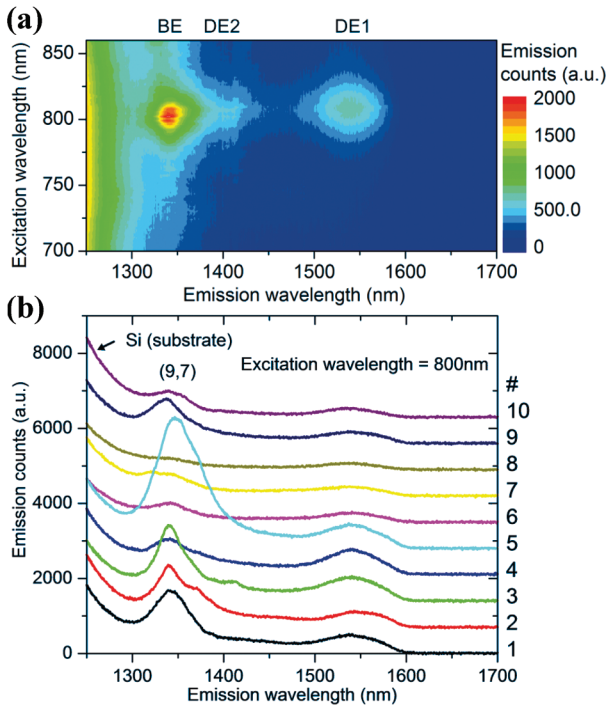

Figure 4. (a) Photoluminescence spectral map of an individual nanotube device (device 3 in (b)) showing the peaks corresponding to a (9,7) SWCNT. (b) Photoluminescence spectra from 10 adjacent devices on a (9,7) SWCNT array, for 800 nm excitation wavelength. Each shows emission at 1345 nm, indicating the presence of a (9,7) SWCNT. Complete spectral maps of the 10 devices are available in Supporting Information. All devices show PL signal, including those that contain nanotubes that are too short to bridge the electrodes and form functioning devices.

with previous predictions and reports of dark excitonic states in SWCNT PL spectra.[27,30] Similar PL spectral maps for 10 adjacent devices from the array are presented in Supporting Information, Figure 4. The emission spectra of these 10 devices at 800 nm excitation are compiled in Figure 4b, showing the bright and dark exciton peaks corresponding to the (9,7) nanotube at all locations. The variation of intensity of the BE peak can be attributed to the orientation of the nanotube with the laser spot and occasional incorporation of multiple nanotubes in the device location. As seen from SEM images, nonbridging nanotubes are often oriented at an angle to the interelectrode direction. In some cases, the minority (8,7) nanotube can also be detected in the gap in the PL spectral map, as seen in Supporting Information, Figure 4. The PL data also confirms the presence of predominantly single-chirality SWCNTs in the high-density device array.

The significant D peak in the Raman spectra measured on these devices indicates the presence of defects in the polymer-wrapped single-chirality SWCNTs.[31] Defects might also be responsible for the large DE peak observed in PL spectra, as has been proposed recently.[32] However, Raman and PL spectra of the same SWCNTs in solution do not show similarly significant D or DE peaks respectively (Figure 5). To exclude the possibility that the dielectrophoretic deposition process itself induces these defects, we prepared control samples where (9,7) SWCNTs were deposited by spin-casting on identical Si/SiO_2 substrates. These macroscopic samples were characterized with a Raman spectrometer at 785 nm excitation, in resonance with the D-mode, G-mode, and RBM Raman scattering processes of the (9,7) SWCNT. Figure 5 shows that the Raman D peak and PL DE peak on spin-casted control samples are indeed very strong compared to SWCNTs in solution and are equally intense as on the DEP assembled devices. The D peak occurs now at 1294 cm^{-1}, just as it is expected to down-shift with the lower excitation energy.[31] We therefore cannot conclusively attribute these peaks to structural defects in the nanotube, because such defects do not appear to exist in nanotubes in suspension and their generation does not depend on the deposition process. The mechanism leading to these defect-related peaks is currently under investigation. Here we report a correlation between the enhanced Raman D peak and the PL DE peak and, in turn, to features in the electron transport characteristics, as shown in the following section.

Electron Transport Measurements. Electron transport measurements on our single-chirality devices show typical nonlinear current−voltage ($I-V$) and p-type transistor characteristics, as expected for Pd-contacted large band gap semiconducting SWCNT FETs,[33] as seen in Figure 6a for a (9,7) nanotube device. However, the On-state current I of a single SWCNT device is typically on the order of 5 nA at a drain-source voltage $V_{DS} = 1$ V. This corresponds to a resistance $R \sim 200$ MΩ, which is large compared to $R \sim 1$ MΩ for similarly fabricated SWCNT FETs from an aqueous surfactant suspension,[9] both on 800 nm thick SiO_2 gate dielectric. We also observe a reduced On/Off ratio of 10^3-10^4 compared to 10^6 expected for polymer-free SWCNT devices. The devices show a subthreshold slope (S) of about 2−5 V/dec,

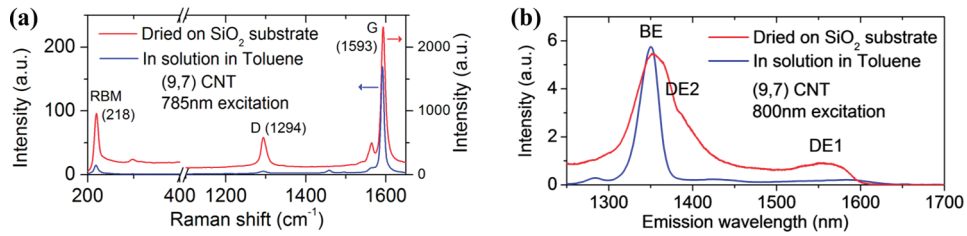

Figure 5. Comparison of (a) Raman and (b) PL spectra of (9,7) SWCNTs dried on a SiO_2 substrate and in solution in toluene showing the enhanced D and DE peaks of the dried nanotubes.

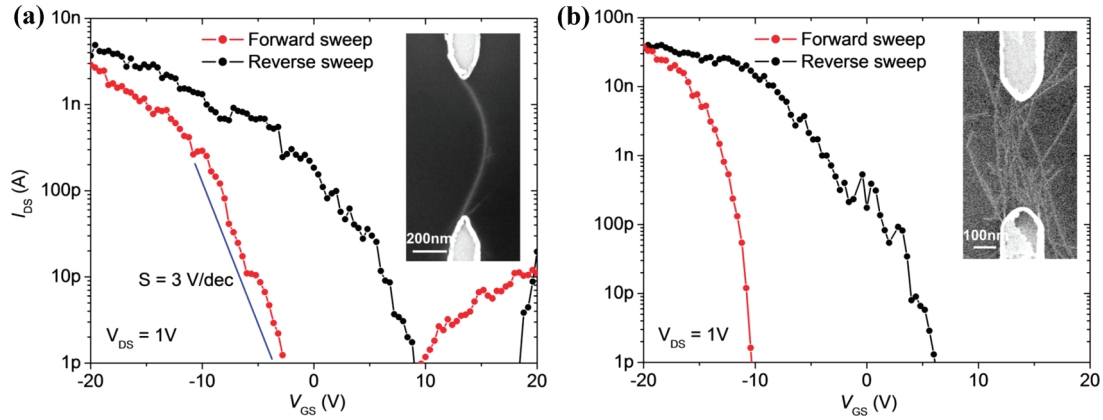

Figure 6. (a) Transistor characteristics of a typical individual (9,7) nanotube device. p-Type characteristics, reduced On-state current, and larger subthreshold slopes (*S*) are typical of such devices. (b) Transistor characteristics of a multiple (9,7) nanotube device consisting of ~5 bridging nanotubes in parallel, showing higher On-state conductance and On/Off ratio. Insets show SEM images of the corresponding devices.

and such slow switching speeds is typical of the thick SiO_2 dielectric. However, similar devices fabricated on 100 nm Al_2O_3 as dielectric also show an $S \sim 2$ V/dec and $R \sim 10$ MΩ. In comparison, the thermal limit of S is $kT \times \ln 10 - 60$ mV/dec The detailed device characteristics of Al_2O_3 dielectric devices will be presented elsewhere. The high resistance, reduced On/Off ratio, and slow switching are most likely due to the polymer wrapping of the SWCNTs. One possible mechanism is that the polymer forms a tunneling barrier at the contact between the metal and the nanotube, which is in addition to the nanotube−metal Schottky barrier. Another explanation is that there is enhanced, polymer-induced carrier scattering along the length of the nanotube. The insensitivity of the nanotube to gate dielectric thickness favors the enhanced scattering model. In fact, enhanced electron scattering has been recently predicted for DNA wrapping around SWCNTs.[34] Such scattering occurs by means of electronic defects[35] and not structural defects. Enhanced scattering at electronic defects could also explain the large D peak in Raman spectra and the DE peak in PL spectra observed in the (9,7) SWCNTs. The fact that these spectral anomalies are not observed for SWCNTs in solution remains a puzzle. The different dielectric environment, *i.e.*, toluene versus air, or interactions with the underlying SiO_2 substrate is suspected to play a role.[36]

The SWCNT device characteristics can be improved by removal of the polymer wrapping and efforts to unwrap the polymer from the SWCNT are currently underway. This is based on our experience with devices deposited from surfactant stabilized aqueous suspensions, where the residual surfactant on the nanotube surface also causes similar reduction in On-state conductance and On/Off ratio.[9] This surfactant, however, can be easily desorbed by annealing at 200 °C.[9] Finally, we note that the observed hysteresis of 10−15 V between forward and reverse sweeps of the gate voltage of ±20 V is smaller than typical values[37] (20−25 V) for as-fabricated SWCNT FETs on an SiO_2 substrate in vacuum. We attribute this to the polymer layer covering each nanotube, similar to the hysteresis suppression by protective polymer[38] or alumina[39] covering. The thin polymer wrapping, however, is not sufficient in itself to entirely suppress hysteresis.

Another advantage of devices fabricated from a single-chirality nanotube source is that multiple nanotubes can be assembled in parallel to improved device performance. We fabricated devices consisting of multiple (5−10) (9,7) nanotubes identical in all other aspects to the single-nanotube devices previously described, resulting in devices with an order of magnitude higher On-state conductance ($I \sim 50$ nA for $V_{DS} = 1$ V) and On/Off ratio (10^4−10^5), as seen in Figure 6b. The flexibility allows us to bridge the performance gap to arc-discharge nanotubes.

CONCLUSIONS

To conclude, we establish the directed assembly of single-chirality carbon nanotubes in high-density device arrays by combining polymer-mediated chirality sorting with dielectrophoretic assembly. This is a major advancement toward the integration of SWCNTs in nanoelectronic circuits, where a narrow distribution in the electronic characteristics among all devices is a prerequisite. Our devices show similar characteristics in PL, Raman, and VC-SEM, as expected for single-chirality devices. However, we also show that the residual polymer wrapping perturbs electron transport through the devices and causes enhanced electron scattering at electronic defects and not structural defects. As evidence, we provide a correlation between electron transport characteristics such as high On-state resistance and insensitivity to gate-oxide thickness, and the Raman and PL spectra that show an enhanced D-mode and DE peak, respectively. We believe that this result is an essential development not only for the wide-

spread application of SWCNTs in optoelectronics, sensing, and nanoelectromechanical systems, but also for cross-correlated interpretation of the results of multiple experimental techniques on a statistically significant number of identical devices. The electronic properties of other nanocarbons, such as double-walled carbon nanotubes and graphene, also depends on chirality[40] and number of layers,[41] respectively. Efforts are underway to sort these into monodisperse suspensions[42] that can subsequently be deposited into monodisperse arrays by dielectrophoresis.[9,43]

MATERIALS AND METHODS

SWCNTs grown by pulsed laser vaporization (PLV) and chemical vapor deposition (HiPCo) processes were suspended in toluene with poly(9,9-di-*n*-octylfluorenyl-2,7-diyl) (POF) by sonication. Due to the selectivity of the polymer to near-armchair chiralities and the low density of toluene, subsequent ultracentrifugation can extract a single chirality of SWCNT. Details of this method can be found in ref 19. In the case of PLV nanotubes, the resultant suspension contains ~90% of (9,7) nanotubes, while HiPCo nanotubes result in a suspension that contains ~50% of (7,5), 25% of (7,6), and 20% of (8,6) nanotubes. Figure 1 shows the PL spectral maps of these two suspensions. The quantitative composition estimates are obtained by the ratio of integrated peak intensity corresponding to different chiralities. This estimate is valid within reasonable error because the fluorescence quantum yields for the nanotubes in question are comparable. A similar composition is also obtained by analysis of absorption spectra. Supporting Information, Figure 1, shows further characterization of the (9,7) suspension, indicating the length distribution and predominance of individual nanotubes in the suspension from the diameter distribution, which is typical of all such suspensions. Additional chiralities can be extracted and enriched using a combination of polymer selectivity and DGU.[44] In comparison, while greater than 99% enrichment in semiconducting SWCNTs can be obtained by DGU in aqueous suspensions,[15] only 80% purity in single-chirality suspensions[45] has been achieved.

High density electrode arrays consisting of 100 devices in a 100 × 100 sq μm area, as shown in Supporting Information, Figure 2, were fabricated by electron-beam lithography. The electrode tips are separated by a 500 nm gap, adjusted according to the mean of the SWCNT length distribution. The electrodes consist of 50 nm Pd with 10 nm Ti adhesion layer on an 800 nm thick insulating thermal SiO_2 layer over a degenerately doped Si back gate. The chirality-sorted nanotubes were deposited from toluene−POF solutions using alternating current (A/C) dielectrophoresis at 2 V/μm peak to peak electric field and 300 kHz frequency. The solution was subsequently rinsed off the array with toluene to remove excess POF residues and dried under a nitrogen flow. We have previously estimated that a concentration of 1 SWCNT per μm^3 in solution is ideal for self-limiting single-nanotube assembly.[9] Multiple-nanotube devices were fabricated by depositing from solution of higher concentration and using higher electric field strength of 3 V/μm.

The SWCNT device arrays were mounted in and wire-bonded to a ceramic package and characterized in a Leo 1530 scanning electron microscope (SEM). The packages are held in a custom sample holder where each leg of the package is individually addressable, to enable combined measurements of electron transport and VC-SEM.[8] VC-SEM was performed under high energy (10 keV) and low dose conditions to minimize charging-related conduction suppression in the nanotube devices. Electron transport was measured under vacuum using an Agilent 4155C semiconductor parameter analyzer.

Raman spectra were recorded with a Witec CRM 200 confocal Raman microscope at room temperature and under inert gas (Ar) flow.[46] Laser irradiation at 633 nm excitation was set to 1 mW power, well below the threshold for nanotube damage. This laser line yields resonant Raman enhancement for the G, D, and RBM lines of the (7,5) nanotube and the G and D lines of the (9,7) nanotube. The laser spot size for the 100× objective, with 6 mm working distance and numerical aperture (NA) of 0.7, is calculated to be 550 nm using the Rayleigh criterion and allows for the measurement of individual nanotube devices in a high-density array that are separated laterally by 3 μm. PL spectral maps were measured using a tunable Ti-Sapphire laser (694−860 nm) at a laser power of 0.6 mW and detected with an InGaAs array (800−1600 nm).[47] This laser line range covers the excitation of the (9,7) nanotube and other potential chiralities in the suspension and devices. The spot-size of the 100× near-infrared objective with a NA of 0.95 was ~1 μm, so individual device spectra can be obtained similar to Raman spectroscopy. Laser polarization in both cases is oriented along the line between the two electrode tips and in parallel to the bridging nanotube. In addition, we prepared control samples of (9,7) SWCNTs in solution and dried by spin-casting, which were characterized with a Kaiser Optical Holospec Raman spectrograph with 785 nm excitation, which yields resonant enhancement for the G, D, and RBM lines of the (9,7) nanotube.[48]

Acknowledgment. The authors acknowledge the assistance of W. Müller. The research was funded by the Initiative and Networking Fund of the Helmholtz-Gemeinschaft Deutscher Forschungszentren (VH-NG-126) and an equipment grant from Agilent Technologies.

Supporting Information Available: Length and diameter distribution and optical absorption spectra of the nanotubes in suspension, optical micrograph of device array, schematic and details of dielectrophoretic deposition, VC-SEM images of an entire array of 100 devices, and photoluminescence spectral maps of 10 adjacent devices. This material is available free of charge *via* the Internet at http://pubs.acs.org.

REFERENCES AND NOTES

1. Dresselhaus, M. S. Nanotechnology: New Tricks with Nanotubes. *Nature* **1998**, *391*, 19–20.
2. Wildoer, J. W. G.; Venema, L. C.; Rinzler, A. G.; Smalley, R. E.; Dekker, C. Electronic Structure of Atomically Resolved Carbon Nanotubes. *Nature* **1998**, *391*, 59–62.
3. McEuen, P. L. Nanotechnology - Carbon-Based Electronics. *Nature* **1998**, *393*, 15–16.
4. Avouris, P. Molecular Electronics with Carbon Nanotubes. *Acc. Chem. Res.* **2002**, *35*, 1026–1034.
5. Zhou, X.; Park, J.-Y.; Huang, S.; Liu, J.; McEuen, P. L. Band Structure, Phonon Scattering, and the Performance Limit of Single-Walled Carbon Nanotube Transistors. *Phys. Rev. Lett.* **2005**, *95*, 146805-1–146805-4.
6. Baughman, R. H.; Zakhidov, A. A.; de Heer, W. A. Carbon Nanotubes - the Route toward Applications. *Science* **2002**, *297*, 787–792.
7. McEuen, P. L. Single-Wall Carbon Nanotubes. *Phys. World* **2000**, *13*, 31–36.
8. Vijayaraghavan, A.; Blatt, S.; Marquardt, C.; Dehm, S.; Wahi, R.; Hennrich, F.; Krupke, R. Imaging Electronic Structure of Carbon Nanotubes by Voltage-Contrast Scanning Electron Microscopy. *Nano Res.* **2008**, *1*, 321–332.
9. Vijayaraghavan, A.; Blatt, S.; Weissenberger, D.; Oron-Carl, M.; Hennrich, F.; Gerthsen, D.; Hahn, H.; Krupke, R. Ultra-Large-Scale Directed Assembly of Single-Walled Carbon Nanotube Devices. *Nano Lett.* **2007**, *7*, 1556–1560.
10. Krupke, R.; Hennrich, F.; von Lohneysen, H.; Kappes, M. M. Separation of Metallic from Semiconducting Single-Walled Carbon Nanotubes. *Science* **2003**, *301*, 344–347.
11. Duesberg, G. S.; Muster, J.; Krstic, V.; Burghard, M.; Roth, S.

Chromatographic Size Separation of Single-Wall Carbon Nanotubes. *Appl. Phys. A: Mater. Sci. Process.* **1998**, *67*, 117–119.
12. Fagan, J. A.; Becker, M. L.; Chun, J. H.; Nie, P. T.; Bauer, B. J.; Simpson, J. R.; Hight-Walker, A.; Hobbie, E. K. Centrifugal Length Separation of Carbon Nanotubes. *Langmuir* **2008**, *24*, 13880–13889.
13. Fagan, J. A.; Becker, M. L.; Chun, J.; Hobbie, E. K. Length Fractionation of Carbon Nanotubes Using Centrifugation. *Adv. Mater.* **2008**, *20*, 1609–1613.
14. Krupke, R.; Hennrich, F.; Weber, H. B.; Kappes, M. M.; von Lohneysen, H. Simultaneous Deposition of Metallic Bundles of Single-Walled Carbon Nanotubes Using Ac-Dielectrophoresis. *Nano Lett.* **2003**, *3*, 1019–1023.
15. Arnold, M. S.; Green, A. A.; Hulvat, J. F.; Stupp, S. I.; Hersam, M. C. Sorting Carbon Nanotubes by Electronic Structure Using Density Differentiation. *Nat. Nanotechnol.* **2006**, *1*, 60–65.
16. Arnold, M. S.; Stupp, S. I.; Hersam, M. C. Enrichment of Single-Walled Carbon Nanotubes by Diameter in Density Gradients. *Nano Lett.* **2005**, *5*, 713–718.
17. Hersam, M. C. Progress Towards Monodisperse Single-Walled Carbon Nanotubes. *Nat. Nanotechnol.* **2008**, *3*, 387–394.
18. Nish, A.; Hwang, J.-Y.; Doig, J.; Nicholas, R. J. Highly Selective Dispersion of Single-Walled Carbon Nanotubes Using Aromatic Polymers. *Nat. Nanotechnol.* **2007**, *2*, 640–646.
19. Hennrich, F.; Lebedkin, S.; Kappes, M. M. Improving Separation Techniques for Single-Walled Carbon Nanotubes: Towards Monodisperse Samples. *Phys. Status Solidi B* **2008**, *245*, 1951–1953.
20. Zheng, M.; Jagota, A.; Strano, M. S.; Santos, A. P.; Barone, P.; Chou, S. G.; Diner, B. A.; Dresselhaus, M. S.; McLean, R. S.; Onoa, G. B.; Samsonidze, G. G.; Semke, E. D.; Usrey, M.; Walls, D. J. Structure-Based Carbon Nanotube Sorting by Sequence-Dependent DNA Assembly. *Science* **2003**, *302*, 1545–1548.
21. Zheng, M.; Jagota, A.; Semke, E. D.; Diner, B. A.; McLean, R. S.; Lustig, S. R.; Richardson, R. E.; Tassi, N. G. DNA-Assisted Dispersion and Separation of Carbon Nanotubes. *Nat. Mater.* **2003**, *2*, 338–342.
22. Engel, M.; Small, J. P.; Steiner, M.; Freitag, M.; Green, A. A.; Hersam, M. C.; Avouris, P. Thin Film Nanotube Transistors Based on Self-Assembled, Aligned, Semiconducting Carbon Nanotube Arrays. *ACS Nano* **2008**, *2*, 2445–2452.
23. Fantini, C.; Jorio, A.; Souza, M.; Strano, M. S.; Dresselhaus, M. S.; Pimenta, M. A. Optical Transition Energies for Carbon Nanotubes from Resonant Raman Spectroscopy: Environment and Temperature Effects. *Phys. Rev. Lett.* **2004**, *93*, 147406-1–147406-4.
24. Oron-Carl, M.; Hennrich, F.; Kappes, M. M.; Lohneysen, H. V.; Krupke, R. On the Electron-Phonon Coupling of Individual Single-Walled Carbon Nanotubes. *Nano Lett.* **2005**, *5*, 1761–1767.
25. Oron, M.; Hennrich, F.; Kappes, M. M.; Krupke, R. Correlation between Transport Measurements and Resonant Raman Spectroscopy on Site-Deposited Individual Carbon Nanotubes. *Electron. Prop. Novel Nanostruct.* **2005**, *786*, 574–577.
26. Piscanec, S.; Lazzeri, M.; Robertson, J.; Ferrari, A. C.; Mauri, F. Optical Phonons in Carbon Nanotubes: Kohn Anomalies, Peierls Distortions, and Dynamic Effects. *Phys. Rev. B* **2007**, *75*, 035427-1–035427-22.
27. Kiowski, O.; Arnold, K.; Lebedkin, S.; Hennrich, F.; Kappes, M. M. Direct Observation of Deep Excitonic States in the Photoluminescence Spectra of Single-Walled Carbon Nanotubes. *Phys. Rev. Lett.* **2007**, *99*, 237402-1–237402-4.
28. Matsunaga, R.; Matsuda, K.; Kanemitsu, Y. Origin of Low-Energy Photoluminescence Peaks in Single Carbon Nanotubes: K-Momentum Dark Excitons and Triplet Dark Excitons. *Phys. Rev. B* **2010**, *81*, 033401-1–033401-4.
29. Torrens, O. N.; Zheng, M.; Kikkawa, J. M. Energy of K-Momentum Dark Excitons in Carbon Nanotubes by Optical Spectroscopy. *Phys. Rev. Lett.* **2008**, *101*, 157401-1–157401-4.
30. Shaver, J.; Kono, J.; Portugall, O.; Krstić, V.; Rikken, G. L. J. A.; Miyauchi, Y.; Maruyama, S.; Perebeinos, V. Magnetic Brightening of Carbon Nanotube Photoluminescence through Symmetry Breaking. *Nano Lett.* **2007**, *7*, 1851–1855.
31. Maultzsch, J.; Reich, S.; Thomsen, C. Chirality-Selective Raman Scattering of the D Mode in Carbon Nanotubes. *Phys. Rev. B* **2001**, *64*, 121407-1–121407-4.
32. Harutyunyan, H.; Gokus, T.; Green, A. A.; Hersam, M. C.; Allegrini, M.; Hartschuh, A. Defect-Induced Photoluminescence from Dark Excitonic States in Individual Single-Walled Carbon Nanotubes. *Nano Lett.* **2009**, *9*, 2010–2014.
33. Chen, Z. H.; Appenzeller, J.; Knoch, J.; Lin, Y. M.; Avouris, P. The Role of Metal-Nanotube Contact in the Performance of Carbon Nanotube Field-Effect Transistors. *Nano Lett.* **2005**, *5*, 1497–1502.
34. Puller, V. I.; Rotkin, S. V. Helicity and Broken Symmetry of DNA-Nanotube Hybrids. *Europhys. Lett.* **2007**, *77*, 27006-p1–27006-p5.
35. Petrov, A. G.; Rotkin, S. V. Transport in Nanotubes: Effect of Remote Impurity Scattering. *Phys. Rev. B* **2004**, *70*, 035408-1–035408-10.
36. Steiner, M.; Freitag, M.; Tsang, J.; Perebeinos, V.; Bol, A.; Failla, A.; Avouris, P. How Does the Substrate Affect the Raman and Excited State Spectra of a Carbon Nanotube. *Appl. Phys. A: Mater. Sci. Process.* **2009**, *96*, 271–282.
37. Vijayaraghavan, A.; Kar, S.; Soldano, C.; Talapatra, S.; Nalamasu, O.; Ajayan, P. M. Charge-Injection-Induced Dynamic Screening and Origin of Hysteresis in Field-Modulated Transport in Single-Wall Carbon Nanotubes. *Appl. Phys. Lett.* **2006**, *89*, 162108-1–162108-3.
38. Kim, W.; Javey, A.; Vermesh, O.; Wang, O.; Li, Y. M.; Dai, H. J. Hysteresis Caused by Water Molecules in Carbon Nanotube Field-Effect Transistors. *Nano Lett.* **2003**, *3*, 193–198.
39. Zavodchikova, M. Y.; Kulmala, T.; Nasibulin, A. G.; Ermolov, V.; Franssila, S.; Grigoras, K.; Kauppinen, E. I. Carbon Nanotube Thin Film Transistors Based on Aerosol Methods. *Nanotechnology* **2009**, *20*, 085201-1–085201-9.
40. Liu, K.; Wang, W.; Xu, Z.; Bai, X.; Wang, E.; Yao, Y.; Zhang, J.; Liu, Z. Chirality-Dependent Transport Properties of Double-Walled Nanotubes Measured in Situ on Their Field-Effect Transistors. *J. Am. Chem. Soc.* **2008**, *131*, 62–63.
41. Partoens, B.; Peeters, F. M. From Graphene to Graphite: Electronic Structure around the K Point. *Phys. Rev. B* **2006**, *74*, 075404-1–075404-11.
42. Green, A. A.; Hersam, M. C. Solution Phase Production of Graphene with Controlled Thickness Via Density Differentiation. *Nano Lett.* **2009**, *9*, 4031–4036.
43. Vijayaraghavan, A.; Dehm, S.; Sciascia, C.; Lombardo, A.; Bonetti, A.; Ferrari, A. C.; Krupke, R. Dielectrophoretic Assembly of High-Density Arrays of Graphene Devices for Rapid Screening. *ACS Nano* **2009**, *3*, 1729–1734.
44. Stürzl, N.; Hennrich, F.; Lebedkin, S.; Kappes, M. M. Near Monochiral Single-Walled Carbon Nanotube Dispersions in Organic Solvents. *The J. Phys. Chem. C* **2009**, *113*, 14628–14632.
45. Kavan, L.; Frank, O.; Green, A. A.; Hersam, M. C.; Koltai, J. n.; Zolyomi, V.; Kuĺti, J.; Dunsch, L. In Situ Raman Spectroelectrochemistry of Single-Walled Carbon Nanotubes: Investigation of Materials Enriched with (6,5) Tubes. *J. Phys. Chem. C* **2008**, *112*, 14179–14187.
46. Hennrich, F.; Krupke, R.; Lebedkin, S.; Arnold, K.; Fischer, R.; Resasco, D. E.; Kappes, M. Raman Spectroscopy of Individual Single-Walled Carbon Nanotubes from Various Sources. *J. Phys. Chem. B* **2005**, *109*, 10567–10573.
47. Lebedkin, S.; Arnold, K.; Hennrich, F.; Krupke, R.; Renker, B.; Kappes, M. M. FTIR-Luminescence Mapping of Dispersed Single-Walled Carbon Nanotubes. *New J. Phys.* **2003**, *5*, 140.1–140.11.
48. Hennrich, F.; Krupke, R.; Arnold, K.; RojasStutz, J. A.; Lebedkin, S.; Koch, T.; Schimmel, T.; Kappes, M. M. The Mechanism of Cavitation-Induced Scission of Single-Walled Carbon Nanotubes. *J. Phys. Chem. B* **2007**, *111*, 1932–1937.